Title

Laurdan Monitors Different Lipids Content in Eukaryotic Membrane During Embryonic Neural Development

Journal

Cell Biochemistry and Biophysics, 70(2)

ISSN

1085-9195

Authors

Bonaventura, Gabriele

Barcellona, Maria Luisa

Golfetto, Ottavia

et al.

Publication Date

2014-11-01

DOI

10.1007/s12013-014-9982-8

Cell Biochem Biophys (2014) 70:785–794
DOI 10.1007/s12013-014-9982-8

ORIGINAL PAPER

Laurdan Monitors Different Lipids Content in Eukaryotic Membrane During Embryonic Neural Development

Gabriele Bonaventura · Maria Luisa Barcellona · Ottavia Golfetto · Jamison L. Nourse · Lisa A. Flanagan · Enrico Gratton

Published online: 17 May 2014

Abstract We describe a method based on fluorescence-lifetime imaging microscopy (FLIM) to assess the fluidity of various membranes in neuronal cells at different stages of development [day 12 (E12) and day 16 (E16) of gestation]. For the FLIM measurements, we use the Laurdan probe which is commonly used to assess membrane water penetration in model and in biological membranes using spectral information. Using the FLIM approach, we build a fluidity scale based on calibration with model systems of different lipid compositions. In neuronal cells, we found a marked difference in fluidity between the internal membranes and the plasma membrane, being the plasma membrane the less fluid. However, we found no significant differences between the two cell groups, E12 and E16. Comparison with NIH3T3 cells shows that the plasma membranes of E12 and E16 cells are significantly more fluid than the plasma membrane of the cancer cells.

Keywords FLIM · mNPSCs · NIH3T3 · Laurdan · Lipid Raft · Membrane fluidity

G. Bonaventura (✉) · M. L. Barcellona
Department of Drug Science, Section of Biochemistry, University of Catania, Catania, Italy
e-mail: gabriele.bonaventura@gmail.com

O. Golfetto · E. Gratton
Laboratory for Fluorescence Dynamics, Department of Biomedical Engineering, University of California, Irvine, California

J. L. Nourse · L. A. Flanagan
Department of Neurology, School of Medicine, University of California, Irvine, California

Introduction

Membrane fluidity changes are implicated in a range of biological processes including signaling, membrane fusion, endocytosis, and many others. Although the role of membrane fluidity during development has been discussed [1–10], a systematic study of changes in membrane fluidity during embryo development has not been carried out. Lipids and lipid domains play a fundamental role in the structural organization of the cytoplasmatic membrane of eukaryotic cells. Lipids in biological membranes are fundamental for the boundary functions of cells, including stimuli to growth and to immunological and stress response, i.e., information delivered from the environment to the cell interior. Membranes of internal organelles allow the compartmentalization of cell functions.

The complexity of the membrane lipid composition has suggested the coexistence of domains characterized by different dynamical properties in the membrane plane as sites for a putative preferential partitioning of proteins and solutes, for modulating membrane activity and for diffusion along the plane and through the bilayer [11–19]. In the last two decades, studies on brain lipids have unequivocally demonstrated that many lipids have critical cell signaling functions [20–26]. They are called "bioactive lipids." Lipid microdomains show high affinity to specific cell signaling proteins such as growth factors or cytokine receptors, which lead to clustering and activation of these receptors [27–34]. These domains are areas in the cell membrane (or intracellular membranes) that arise from the self-assembly of lipids in an ordered (Lo) structure in the liquid phase of the membrane. The lipid raft hypothesis has had a wide impact on the field of cellular biology, especially in neural cells as functional membrane domains for cell–cell interactions and signal transduction [20–26]. The

minimum lipid composition of a raft is cholesterol and sphingomyelin, which is associated with glycerolsphingolipids (GSLs) or with a glycerolphospholipid such as phosphatidylcholine. Glycerophospholipids, cholesterol, and the sphingolipid backbone ceramide are synthesized at the ER. Considering the bidirectional vesicular connection between the ER and the plasma membrane, the most remarkable feature of the lipid organization in mammalian cells is the enrichment of sphingolipids and cholesterol in the late Golgi, plasma membrane, and endosomes. Cholesterol spontaneously moves between and across membranes as a monomer. Its location is determined by its high affinity for sphingolipids and saturated glycerophospholipids. The composition and concentration of gangliosides, or sialic acid-containing GSLs, change dramatically during central nervous system (CNS) development. This change in the composition of gangliosides is correlated with defined developmental events and is evolutionarily conserved among many mammalian species [35–41]. In general, during CNS development, the composition of GSLs begins with a relatively simple pattern, with GM3 and GD3 predominating in early neuroectoderm. This pattern is soon followed by the transient appearance of c-series gangliosides during the period of neural tube formation, followed by a more complex pattern, with four gangliosides of the a- and b-series, GM1, GD1a, GD1b, and GT1b. These latter complex gangliosides constitute the major gangliosides in mature brain [35–41]. Subcellular localization studies revealed that GM1 and GD1a are localized mainly on the plasma membrane and partly in the cytoplasm, both as punctate clusters. This punctate distribution suggests localization of GM1 and/or GD1a in specialized structures, such as membrane microdomains.

It has been suggested that in mammalian neural cells, membrane lipid rafts could serve as key assembly and sorting platforms for cell–cell interactions or signal transduction complexes and modulate multiple cellular processes, such as axonal growth and guidance for neuronal growth cones, cytokine/growth factor receptor signaling, neuron/glia interactions, neuronal survival and death, and many more [28, 42–48].

Apart from invasive methods that use membrane isolation, which does not allow real-time in situ measurements and may lead to artifacts because lipids can migrate between different cellular compartments during the membrane isolation, fluorescence spectroscopy is one of the most commonly used tools for the investigation of lipid dynamical properties. The information on membrane packing and dynamics is obtained from the spectroscopic properties of fluorescent probes in the membrane such as excitation and emission spectra, polarization, and lifetime. Among several fluorescent probes, the sensitivity of 2-dimethylamino-6-lauroylnaphthalene (Laurdan) to the polarity of the membrane environment presents several advantages for membrane studies [49–52]. This sensitivity arises from the greater than 50-nm red shift of the emission maximum in polar versus nonpolar environments, so that simple fluorescence intensity measurements at two properly selected wavelengths provide information on the membrane polarity. Several studies have shown that Laurdan spectroscopic properties reflect local water content in the membrane [53–60] and indirectly, membrane fluidity. Laurdan is a molecule whose spectroscopic properties are influenced by both the composition and dynamics of its local surroundings [61–63]. In other words, Laurdan's fluorescence properties are dependent on two major factors: the polarity of the environment (ground state of the fluorophore) and the rate of dipolar relaxation of molecules or molecular residues that can reorient around Laurdan's fluorescent moiety during its excited-state lifetime [64, 65].

In this work, we propose a detection scheme that isolates different wavelength bands of Laurdan's emission in such a way that changes in polarity (ground state) are detected independently on changes in dipolar relaxation (excited state). Using fluorescence-lifetime imaging microscopy (FLIM) and analyzing the data with the phasor approach, we first acquired the fluorescence decay at each pixel of an image and then we applied the phasor transformation to the decay measured at each pixel. The transformed points (two coordinates for each pixel of the image) are then plotted on the phasor plot. We report the analysis of the fluorescence decay of Laurdan as a tool to detect changes in membrane lipid packing in live cell membranes, based on polarity and dipolar relaxations. In the phasor plot, different trajectories for changes in polarity versus changes in cholesterol content are visualized [66–69]. This analytical procedure gives the ability to investigate in vivo membranes with different properties such as water content and cholesterol content and thus to perform a more comprehensive analysis of cell-membrane heterogeneity during development [49–70].

Our results on neural precursor cells from mouse embryos at different stages of development (E12 and E16 day of gestation) show that there are at least two independent causes that determine the direction of changes in the phasor location. One is the polarity of the environment (which changes the true lifetime), and the other is the capability of water to give rise to the dipolar relaxation phenomenon (which moves the phasor distribution outside of the universal circle). Therefore, using Laurdan's lifetime decay in two detection channels (*blue and green*), we can disentangle the effects of polarity from dipolar relaxations due to addition/subtraction of cholesterol, giving us unprecedented details about cholesterol and heterogeneous distribution of polarity/fluidity in cell membranes.

Methods

Primary Cell Culture

Pregnant wild-type CD1+ mice were used for obtaining embryos at E12 and E16. Cerebral cortices were dissected and the dissociated cells passed through a sterile nylon sieve (82 μm pores) and then pooled and seeded in culture dishes to generate cultures of mouse fetal-derived neural stem/precursor cells (NSPCs).

Cultures of NSPCs were grown floating in suspension as neurospheres in Dulbecco's modified Eagle's medium with B27, N2, 1 mM sodium pyruvate, 2 mM glutamine, 1 mM *N*-acetylcysteine (Sigma-Aldrich, St. Louis, USA), 20 ng/ml epidermal growth factor, (EGF), (BD Biosciences, Bedford, MA, USA), 10 ng/ml fibroblast growth factor, (FGF) (BD Biosciences, Bedford, MA, USA), and 2 μg/ml heparin (Sigma-Aldrich St. Louis, IN, USA).

All chemical reagents were from Gibco (Invitrogen, Grand Island, NY, USA) unless otherwise specified and of the highest purity available. Neurospheres are a heterogeneous collection of cells that includes a small number of stem cells, a greater number of more specified progenitor cells, and a few differentiated cells such as astrocytes and neurons. Neurospheres were dissociated using NeuroCult medium kit (Stem Cell Technologies, Vancouver, Canada), and the resulting individual cells were plated on laminin-coated glass bottom dishes and adhered for 24 h prior to FLIM analysis.

NIH3T3 Cell Cultures

NIH/3T3 (mouse fibroblast) cell line was purchased from Sigma-Aldrich. The cells were cultured in Dulbecco's Modified Eagle's Medium (DMEM), supplemented with 1.5 g/L sodium bicarbonate, 10 mM HEPES, pH 7.4, 100 U/mL penicillin G, 100 L/g/mL streptomycin, and 10 % fetal calf serum at 37 °C in a humidified atmosphere consisting of 95 % air and 5 % CO_2. Cells were passaged by removing 90 % of the supernatant and replacing it with fresh medium approximately twice a week and detachment using a 0.25 % trypsin-EDTA solution. For FLIM experiments, the cells were scraped and plated on glass bottom dishes (MatTeck, AshLand, U.S.A.) coated with 10 μg/ml poly-D-lysine (MP Biomedicals, California, U.S.A.) and 20 μg/ml laminin (Sigma-Aldrich), 1 day prior the analysis.

FLIM Analysis

FLIM data were acquired with a Zeiss LSM710 META Laser scanning microscope, coupled to a 2-Photon Ti:Sapphire laser (Spectra-Physics Mai Tai, Newport Beach, CA) producing 80 fs pulses at a repetition of 80 MHz and a ISS A320 FastFLIMBox for the lifetime data. A 40× water immersion objective 1.2 N.A. (Zeiss, Oberkochen, Germany) was used for all experiments. The excitation wavelength was set at 780 nm. A SP 760-nm dichroic filter was used to separate the fluorescence signal from the laser light. For FLIM data, the fluorescence signal was directed through a 495 LP filter and the signal was split between two photo-multiplier detectors (H7422P-40, Hamamatsu, Japan), with the following bandwidth filters in front of each: blue channel 460/40 and green 540/25, respectively. For image acquisition, the pixel frame size was set to 256 × 256 and the pixel dwell time was 25.61 μs/pixel. The average laser power at the sample was maintained at the mW level.

The Phasor Transformation and its Interpretation

In a FLIM measurement, the fluorescence decay is obtained at each pixel generally using a photon counting system that measures the histograms of time delays between the excitation of the molecule due to the laser pulse excitation and the emission of a photon from the excited state of the molecule. In each pixel, an average of about 100–500 photons is collected. Analysis of the decay using exponential models cannot be done accurately using such a low number of photons in the histogram, and specifically for Laurdan, an exponential decay is inadequate to describe the decay since Laurdan decay is affected by excited-state reactions. In the phasor approach, only few moments of the delay histogram are used to determine some proprieties of the decay. The phasor approach applies a transformation (the phasor transformation) to the measured decay histogram as shown in Eqs. 1 and 2, where $I_{ij}(t)$ is the histogram of photon delays measured at pixel (i,j). At each pixel, the phasor transformation provides two coordinates g and s, which are plotted in a polar plot called the phasor plot.

$$g_{i,j}(\omega) = \frac{\int_0^T I_{i,j}(t)\cos(\omega t)\mathrm{d}t}{\int_0^T I_{i,j}(t)\mathrm{d}t} \quad (1)$$

$$s_{i,j}(\omega) = \frac{\int_0^T I_{i,j}(t)\sin(\omega t)\mathrm{d}t}{\int_0^T I_{i,j}(t)\mathrm{d}t} \quad (2)$$

There is a relationship between the exponential decay and points in the phasor plot (Fig. 1). If the fluorescence decay is single exponential, the phasor transformation gives points that lay on a semicircle called the universal circle.

The phasor transformation has the property that the coordinates g and s behave like coordinates of a vector. The consequence of this mathematical property is that if in

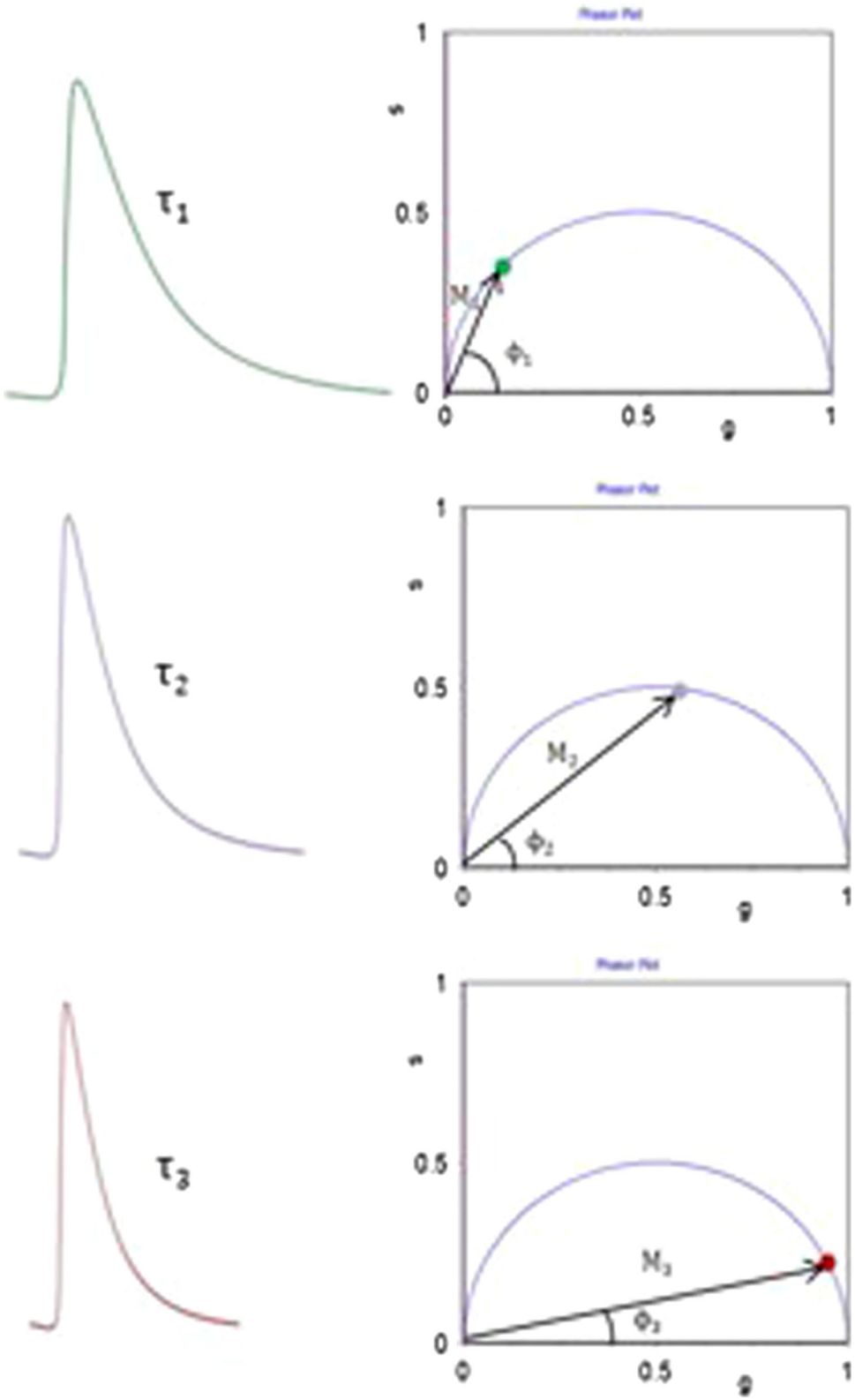

Fig. 1 Schematic of the phasor transformation. Decay curves with different single-exponential lifetime map in different position in the phasor plot with points on the universal circle. The faster is the exponential decay, the more the point is to the right

a pixel we have molecules that decay with two different exponential constants, the phasor of each of the molecules will lay on different points on the universal circle, but their linear combination (which depends on their fractional intensity contribution to the decay in that pixel) must be on the line joining the two points on the universal circle, as

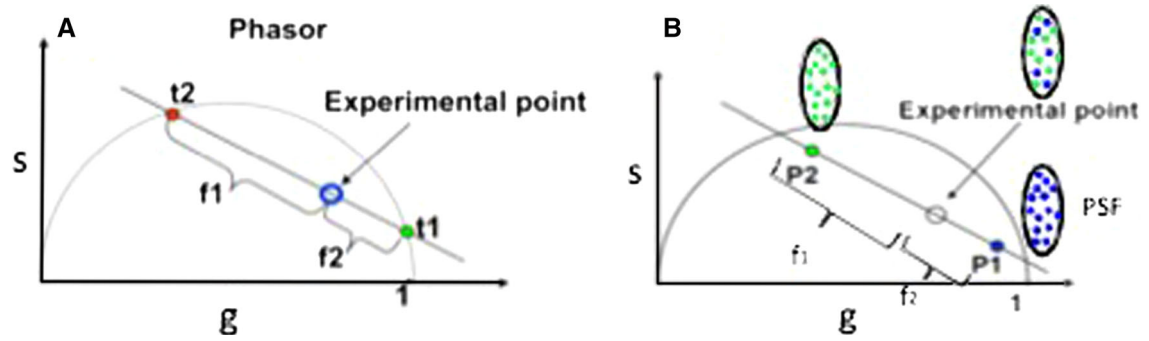

Fig. 2 Linear combination property of phasors. **a** The combination in one pixel of two single exponentials gives a phasor value on the line joining the phasors corresponding to the two exponentials. **b** If in one pixel (the size of the PSF, about 300 nm) there are Laurdan molecules with different environments, although each environment is decaying as a complex exponential, they will combine linearly to give experimental points in the line joining the phasors of the two different environments

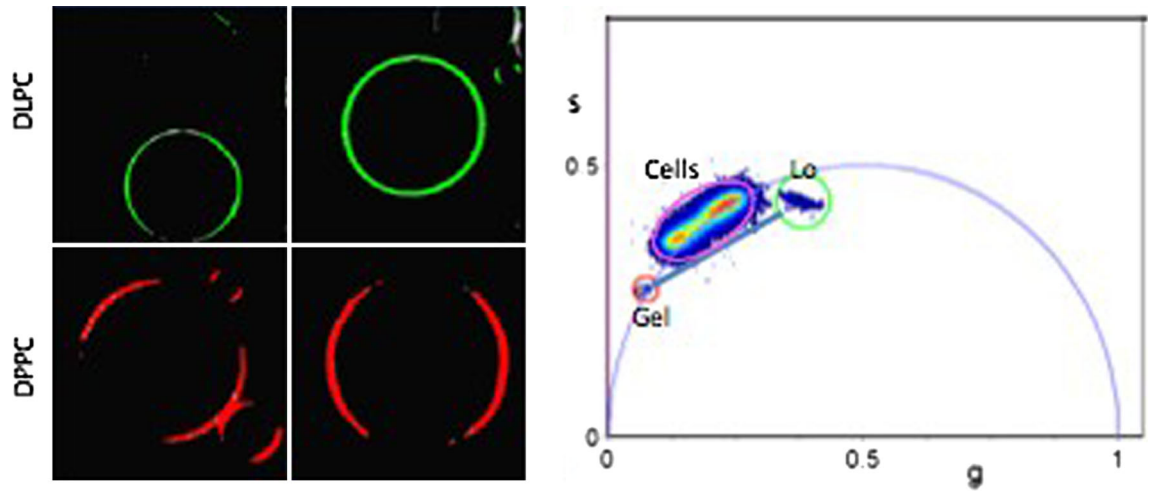

Fig. 3 Empirical sensitivity scale for Laurdan in two extreme phases, gel and liquid crystalline. The *red* cursor marks the position of the gel phase as found in the GUVs at room temperature, and the *green* cursor corresponds to the phasor position of DLPC at room temperature, which is in the liquid-disordered phase. Note that the cell values (E12 and E16 cells) are not on the linear combination line of these two extreme values but they lay on or close to the universal circle indicating that the cell membrane is quite different than the pure phospholipid phases (Color figure online)

shown in Fig. 2a. This linear combination property holds even for the phasors of the two species that are not on the universal circle (Fig. 2b). Since the decay of Laurdan is nonexponential, if in one pixel we have coexistence of regions of different decay properties, the measured phasor must be on the line corresponding to these different decay properties. For example, if in one pixel we have coexistence of regions (microdomains below the pixel resolution) of liquid order and liquid disorder, then the phasor position must be along the line joining the phasor of the liquid order and liquid-disordered membrane phases (Fig.3).

Sensitivity to Membrane Fluidity Changes

To establish an empirical scale of fluidity, we measured the phasor positions of Laurdan in an artificial system composed of two different lipids that at the same temperature form two different phases, liquid and gel. Of course, we do not expect these two phases to exist in biological systems, but we are using this scale as an indication of the maximum range of changes expected in lipid bilayer systems.

Results

FLIM images were collected for the E12, E16, and a control group of NIH3T3 cells. Figure 4 shows a typical phasor plot analysis for E12 and E16 (N = 8cells).

The red cursor selects pixels with more rigid membranes while the green cursor selects more fluid regions. The statistical analysis of all cells measured and of the NIH3T3 control group is shown in Table 1. There is a

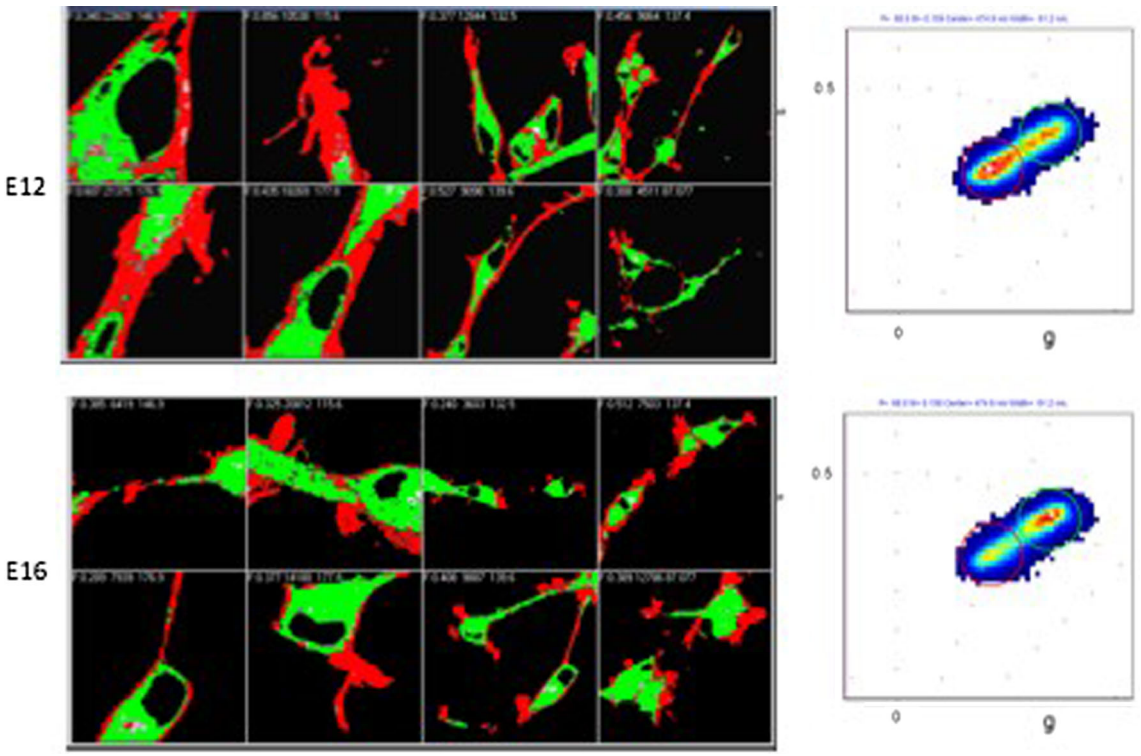

Fig. 4 Phasor analysis of E12 and E16 cells (Channel 1). The compound phasor plot for each group (E12 and E16) is shown at right. For this analysis, the position of the *red* and *green* cursor selectors was not changed. For each cell, the number of pixels in the *red* and *green* cursor was recorded. The results of the average number of pixels and the significance of the observed difference are shown in Table 1 (Color figure online)

Table 1 Number of pixel recorded in red and green cursor

	R1	G1	G1/R1	R2	G2	G2/R2
E12 (N = 8)	0.488/0.178	0.371/0.150	0.76 p0.25	0.262/0.122	0.447/0.146	1.70 p0.25
E16 (N = 8	0.381/0.085	0.437/0.119	1.15–	0.207/0.049	0.375/0.073	1.81–
NIH3T3 (N = 20)	0.488/0.086	0.284/0.076	0.57 p0.01	0.309/0.061	0.271/0.056	0.87 p0.01

Results of the average number of pixels and their significance

clear separation between the red- and the green-colored pixels, with the red pixels preferentially localized on the plasma membrane. As shown in the statistical analysis in Table 1, there is no significant difference between the relative fraction of red- and green-colored pixels for the two groups E12 and E16, while there is a significant difference between the NIH3T3 cell groups shown in Fig. 2.

Also, for the NIH3T3 cells, the red-colored pixels are prevalent in the plasma membrane (Fig. 5). However, the NIH3T3 cells show a larger fraction of red pixels which are associated with the plasma membranes, which could be attributed to different state of development of these cells compared to the E12 and E16 with more rigid external membranes.

So far, we have investigated the statistics of pixels corresponding to the red and green cursor selection. The question remains in regard to the distribution of pixels in the plasma membrane alone rather than in the plasma membrane and in the internal membranes. This separation requires selection of pixels in the plasma membrane and a proper statistical evaluation of the fluidity at these pixels. For this purpose, we generated a mask based on intensity selection which mainly selects pixels with high concentration of the Laurdan probe. Figure 6 shows the mask with two color cursors which divide the regions, which previously (in Fig. 4) was selected by the red cursor (more rigid, selecting the plasma membrane). The statistics of pixels in the two sub-cursors again shows no significant difference between the E12 and E16 cells (p value = 0.78).

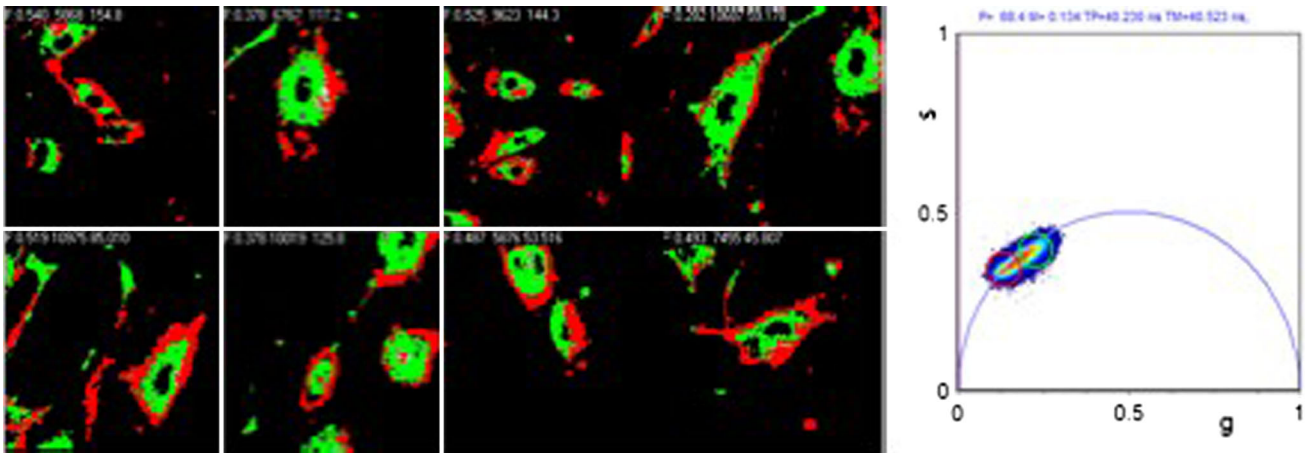

Fig. 5 Phasor analysis of NIH3T3 cells. The positions of the *red* and *green* cursor selectors are the same as in Fig. 1. The statistics of the pixels in each of the cursors is shown in table 1. The fraction of *green*-colored pixels is larger for the group of (N = 20) NIH3T3 cells than for the neuronal cells (Color figure online)

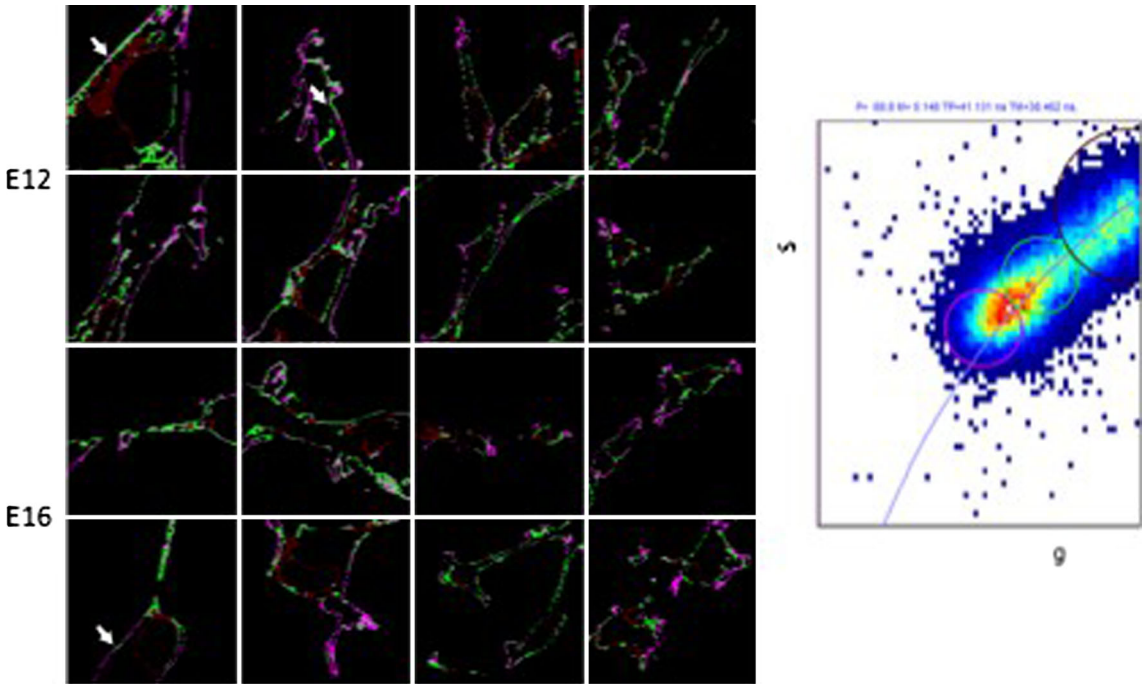

Fig. 6 Selection of pixels with prevalent distribution in the plasma membrane. The *red* cursor selection in Fig. 1 was subdivided in two parts using the *pink* and *green* cursor. The *green* cursor in Fig. 1 was substituted with a *black* cursor, effectively painting in *black* all pixels of high fluidity. The statistical analysis of the pixels painted with the two different colors show no significant difference between the two groups of cells (E12 and E16). The *white* arrows indicate some regions along the plasma membrane of apparent different fluidity (Color figure online)

Discussion

In this work, we explored a method to measure the fluidity of membranes with very high spatial resolution and with high sensitivity to membrane fluidity. The spatial resolution (in the order of 1–2 pixels, about 300 nm) is needed to separate the contribution of the plasma membrane from that of internal membranes. In all type of cell measured, we found that the plasma membrane is more rigid than internal membranes and that for the cell line NIH3T3 the plasma membrane is more rigid compared to the E12 and E16 cells. Although one of the purposes of this investigation was to establish if the fluidity of the plasma membrane of neuronal cells changes at different gestation days, we found

that there is no significant change. This conclusion could depend on the S/N ratio which does not allow sufficient separation of pixel in the fluidity scale. However, we were able to detect a significantly different spatial organization of the membranes according to their fluidity index with the plasma membrane being always more rigid than the internal membranes. This difference presumably is a reflection of the expected different lipid composition of the membranes in neuronal cells, as well as in all other type of cells. The plasma membrane in many types of cells has a lipid composition very different from that of the internal membranes. Cellular membranes contain glycerophospholipids, comprising one of the several head groups attached via glycerol to two acyl chains, one of which is usually unsaturated. Although glycerophospholipids are sufficient to form bilayers, most eukaryotic cells, like neurons, contain two additional classes of lipids: sterols and sphingolipids. The sterols are based on a rigid four-ring structure, with cholesterol being the principle form found in vertebrates. Sterols and sphingolipids are present at low levels in internal membranes and indeed are synthesized in the endoplasmic reticulum (ER) and Golgi, respectively, but are at high levels in the plasma membrane and endosome [71, 72]. Along the plasma membrane, we can notice regions of distinct fluidity (see for example Fig. 6). This can be due to relatively large regions of different lipid composition or to the proximity in these pixels of internal membranes that have a different fluidity. We would like to stress that cellular membranes contain hundreds of lipid species that differ in their polar headgroups and fatty tails. But, even if the matrix of cellular membranes is the classic fluid lipid bilayer, the vesicular transport is bidirectional and fast as compared to the turnover of membrane components. One important question now arises: how cells maintain the identities of the membranes of their organelles. Remarkably, in the endoplasmic reticulum (ER) and in the other membrane fluidized by cholesterol, the different mutual affinities of lipids generally unsaturated and saturated can yield coexisting lipid phases of different fluidity (i.e., liquid-ordered vs. disordered). Because of its high levels of unsaturated lipids and low levels of sphingolipids and cholesterol, the ER membrane is highly flexible with a high rate of spontaneous transbilayer lipid translocation.

By comparing the results obtained with the NIH3T3 cells versus the mouse neural stem/precursor cells (mNPSCs) at different stage of prenatal development (E12 and E16), cellular membranes in the mouse fibroblast NIH3T3 appear to be more rigid. This result is justified by the highly defined competence of the fibroblasts devoted to a structural function, exemplified by a branched cytoplasm surrounding an elliptical, speckled nucleus having two or more nucleoli.

The size of microdomains (rafts) is predicted to be below the resolution of our microscope so that the observation of relatively large regions in the plasma membrane (see Fig. 6, regions marked by white arrows) of different fluidity should be further investigated. In conclusion, Laurdan has sufficient sensitivity to separate different membranes in neuronal cells typically internal membranes from external membranes. With respect to development of neuronal cells, we have not observed significant changes between the E12 and E16 groups in regard to overall changes in membrane fluidity. This result could indicate that at this stage of development, the membrane of neuronal cells is already organized or that the S/N ratio provided by the phasor-FLIM technique is insufficient to detect subtle changes in membrane composition.

Acknowledgments Funding was provided by National Institutes of Health P50 GM076516, 5P41RR003155-27-8 P41 GM103540-27 (EG and OG), and UL1 TR000153 from the National Center for Research Resources (NCRR), a component of the National Institutes of Health (NIH) and the NIH Roadmap for Medical Research. GB and MB acknowledge funds from the Italian Ministry of University and Research MIUR 2012/13 PhD Neurobiology, Department of Chemical Sciences, University of Catania, Italy.

References

1. Los, D. A., Mironov, K. S., & Allakhverdiev, S. I. (2013). Regulatory role of membrane fluidity in gene expression and physiological functions. *Photosynthesis research, 116*(2–3), 489–509.
2. Wiśniewska, A., Draus, J., & Subczynski, W. K. (2003). Is a fluid-mosaic model of biological membranes fully relevant? Studies on lipid organization in model and biological membranes. *Cellular & Molecular Biology Letters, 8*(1), 147–159.
3. Wang, T. Y., & Silvius, J. R. (2003). Sphingolipid partitioning into ordered domains in cholesterol-free and cholesterol-containing lipid bilayers. *Biophysical Journal, 84*(1), 367–378.
4. Lin, C., Wang, L. H., Fan, T. Y., & Kuo, F. W. (2012). Lipid content and composition during the oocyte development of two gorgonian coral species in relation to low temperature preservation. *PLoS One, 7*(7), e38689.
5. Marguet, D., Lenne, P. F., Rigneault, H., & He, H. T. (2006). Dynamics in the plasma membrane: How to combine fluidity and order. *EMBO Journal, 25*(15), 3446–3457.
6. Weeks, G., & Herring, F. G. (1980). The lipid composition and membrane fluidity of Dictyostelium discoideum plasma membranes at various stages during differentiation. *Journal of Lipid Research, 21*(6), 681–686.
7. Nozawa, Y., Kasai, R., Kameyama, Y., & Ohki, K. (1980). Age-dependent modifications in membrane lipids: Lipid composition, fluidity and palmitoyl-CoA desaturase in Tetrahymena membranes. *Biochimica et Biophysica Acta, 599*(1), 232–245.
8. Quinn, P. J., & Chapman, D. (1980). The dynamics of membrane structure. *CRC Critical Reviews In Biochemistry, 8*(1), 1–117. Review.
9. Hitzemann, R. J., & Johnson, D. A. (1983). Developmental changes in synaptic membrane lipid composition and fluidity. *Neurochemical Research, 8*(2), 121–131.
10. Hashimoto, M., Hossain, S., & Masumura, S. (1999). Effect of aging on plasma membrane fluidity of rat aortic endothelial cells. *Experimental Gerontology, 34*(5), 687–698.

11. Maurya, S. R., Chaturvedi, D., & Mahalakshmi, R. (2013). Modulating lipid dynamics and membrane fluidity to drive rapid folding of a transmembrane barrel. *Scientific Reports, 3*, 1989.
12. Bakht, O., Pathak, P., & London, E. (2007). Effect of the structure of lipids favoring disordered domain formation on the stability of cholesterol-containing ordered domains (lipid rafts): Identification of multiple raft-stabilization mechanisms. *Biophysical Journal, 93*(12), 4307–4318.
13. Fan, J., Sammalkorpi, M., & Haataja, M. (2010). Lipid microdomains: structural correlations, fluctuations, and formation mechanisms. *Physical Review Letters, 104*(11), 118101.
14. Martinez-Seara, H., Róg, T., Pasenkiewicz-Gierula, M., Vattulainen, I., Karttunen, M., & Reigada, R. (2008). Interplay of unsaturated phospholipids and cholesterol in membranes: Effect of the double-bond position. *Biophysical Journal, 7*, 3295–3305.
15. Ayuyan, A. G., & Cohen, F. S. (2008). Raft composition at physiological temperature and pH in the absence of detergents. *Biophysical Journal, 94*(7), 2654–2666.
16. Sengupta, P., Baird, B., & Holowka, D. (2007). Lipid rafts, fluid/fluid phase separation, and their relevance to plasma membrane structure and function. *Seminars in Cell & Developmental Biology, 5*, 583–590. Review.
17. Niemelä, P. S., Ollila, S., Hyvönen, M. T., Karttunen, M., & Vattulainen, I. (2007). Assessing the nature of lipid raft membranes. *PLoS Computational Biology, 3*(2), e34.
18. Gallegos, A. M., Storey, S. M., Kier, A. B., Schroeder, F., & Ball, J. M. (2006). Structure and cholesterol dynamics of caveolae/raft and non raft plasma membrane domains. *Biochemistry, 45*(39), 12100–12116.
19. Wassall, S. R., Brzustowicz, M. R., Shaikh, S. R., Cherezov, V., Caffrey, M., & Stillwell, W. (2004). Order from disorder, corralling cholesterol with chaotic lipids. The role of polyunsaturated lipids in membrane raft formation. *Chemistry and Physics of Lipids, 132*(1), 79–88.
20. Kusumi, A., & Suzuki, K. (2005). Toward understanding the dynamics of membrane-raft-based molecular interactions. *Biochimica et Biophysica Acta, 1746*(3), 234–251. Review.
21. Jasmin, J. F., Yang, M., Iacovitti, L., & Lisanti, M. P. (2009). Genetic ablation of caveolin-1 increases neural stem cell proliferation in the subventricular zone (SVZ) of the adult mouse brain. *Cell Cycle, 8*, 3978–3983.
22. Fields, R. D., Black, J. A., & Waxman, S. G. (1987). Filipin-cholesterol binding in CNS axons prior to myelination: Evidence for microheterogeneity in premyelinated axolemma. *Brain Research, 404*, 21–32.
23. Yanagisawa, M., Nakamura, K., & Taga, T. (2005). Glycosphingolipid synthesis inhibitor represses cytokine-induced activation of the Ras-MAPK pathway in embryonic neural precursor cells. *Journal of Biochemistry, 138*, 285–291.
24. Suetake, K., Liour, S. S., Tencomnao, T., & Yu, R. K. (2003). Expression of gangliosides in an immortalized neural progenitor/stem cell line. *Journal of Neuroscience Research, 74*, 769–776.
25. Yu, R. K., Macala, L. J., Taki, T., Weinfield, H. M., & Yu, F. S. (1988). Developmental changes in ganglioside composition and synthesis in embryonic rat brain. *Journal of Neurochemistry, 50*, 1825–1829.
26. Yu, R. K., Nakatani, Y., & Yanagisawa, M. (2009). The role of glycosphingolipid metabolism in the developing brain. *Journal of Lipid Research, 50*, 440–445.
27. Barenholz, Y. (2002). Cholesterol and other membrane active sterols: From membrane evolution to "rafts". *Progress in Lipid Research, 41*(1), 1–5. Review.
28. Hla, T., Lee, M. J., Ancellin, N., Paik, J. H., & Kluk, M. J. (2001). Lysophospholipids–receptor revelations. *Science, 294*, 1875– 1878.
29. Radeff-Huang, J., Seasholtz, T. M., Matteo, R. G., & Brown, J. H. (2004). G protein mediated signaling pathways in lysophospholipid induced cell proliferation and survival. *Journal of Cellular Biochemistry, 92*, 949–966.
30. Mukhopadhyay, A., Saddoughi, SA., Song, P., Sultan, I., Ponnusamy, S., Senkal, CE., Snook, CF., Arnold, HK., Sears, RC., Hannun, YA., & Ogretmen, B. (2008). Direct interaction between the inhibitor 2 and ceramide via sphingolipid-protein binding is involved in the regulation of protein phosphatase 2A activity and signaling. *The FASEB Journal.*
31. Basu, S., Bayoumy, S., Zhang, Y., Lozano, J., & Kolesnick, R. (1998). BAD enables ceramide to signal apoptosis via Ras and Raf-1. *Journal of Biological Chemistry, 273*, 30419–30426.
32. Yin, X., Zafrullah, M., Lee, H., Haimovitz-Friedman, A., Fuks, Z., & Kolesnick, R. (2009). A ceramide-binding C1 domain mediates kinase suppressor of ras membrane translocation. *Cellular Physiology and Biochemistry, 24*, 219–230.
33. Bourbon, N. A., Yun, J., & Kester, M. (2000). Ceramide directly activates protein kinase C zeta to regulate a stress-activated protein kinase signaling complex. *Journal of Biological Chemistry, 275*, 35617–35623.
34. Krishna, S., & Zhong, X. P. (2013). Regulation of lipid signaling by diacylglycerol kinases during T cell development and function. *Frontiers in Immunology, 4*, 178.
35. Hirabayashi, Y., Hirota, M., Suzuki, Y., Matsumoto, M., Obata, K., & Ando, S. (1989). Developmentally expressed *O*-acetyl ganglioside GT3 in fetal rat cerebral cortex. *Neuroscience Letters, 106*, 193–198.
36. Yu, R. K. (1994). Development regulation of ganglioside metabolism. *Progress in Brain Research, 101*, 31–44. Review.
37. Rösner, H., al-Aqtum, M., & Rahmann, H. (1992). Gangliosides and neuronal differentiation. *Neurochemistry International, 20*(3), 339–351.
38. Kotani, M., Terashima, T., & Tai, T. (1995). Developmental changes of ganglioside expressions in postnatal rat cerebellar cortex. *Brain Research, 700*(1–2), 40–58.
39. Letinić, K., Heffer-Lauc, M., Rosner, H., & Kostović, I. (1998). C-pathway polysialogangliosides are transiently expressed in the human cerebrum during fetal development. *Neuroscience, 86*(1), 1–5.
40. Liour, S. S., Kapitonov, D., & Yu, R. K. (2000). Expression of gangliosides in neuronal development of P19 embryonal carcinoma stem cells. *Journal of Neuroscience Research, 62*(3), 363–373.
41. Giménez, C. (1998). Composition and structure of the neuronal membrane: Molecular basis of its physiology and pathology. *Revista de Neurologia, 26*(150), 232–239. Review.
42. Chen, L., & Khillan, J. S. (2010). A novel signaling by vitamin A/retinol promotes self renewal of mouse embryonic stem cells by activating PI3 K/Akt signaling pathway via insulin-like growth factor-1 receptor. *Stem Cells, 28*, 57–63.
43. Lewis, P. M., Dunn, M. P., McMahon, J. A., Logan, M., Martin, J. F., St-Jacques, B., et al. (2001). Cholesterol modification of sonic hedgehog is required for long-range signaling activity and effective modulation of signaling by Ptc1. *Cell, 105*, 599–612.
44. Lee, M. Y., Ryu, J. M., Lee, S. H., Park, J. H., & Han, H. J. (2010). Lipid rafts play an important role for maintenance of embryonic stem cell self-renewal. *Journal of Lipid Research, 51*, 2082–2089.
45. Meyer zu Heringdorf, D., & Jakobs, K. H. (2007). Lysophospholipid receptors: signalling, pharmacology and regulation by lysophospholipid metabolism. *Biochimica et Biophysica Acta, 1768*, 923–940.
46. Gardell, S. E., Dubin, A. E., & Chun, J. (2006). Emerging medicinal roles for lysophospholipid signaling. *Trends in Molecular Medicine, 12*, 65–75.

47. Hla, T., Lee, M. J., Ancellin, N., Thangada, S., Liu, C. H., Kluk, M., et al. (2000). Sphingosine-1-phosphate signaling via the EDG-1 family of G-protein-coupled receptors. *Annals of the New York Academy of Sciences, 905*, 16–24.
48. Okudaira, S., Yukiura, H., & Aoki, J. (2010). Biological roles of lysophosphatidic acid signaling through its production by autotaxin. *Biochimie, 92*, 698–706.
49. Golfetto, O., Hinde, E., & Gratton, E. (2013). Laurdan fluorescence lifetime discriminates cholesterol content from changes in fluidity in living cell membranes. *Biophysical Journal, 104*(6), 1238–1247.
50. Hofstetter, S., Denter, C., Winter, R., McMullen, L. M., & Gänzle, M. G. (2012). Use of the fluorescent probe LAURDAN to label and measure inner membrane fluidity of endospores of *Clostridium* spp. *Journal of Microbiol Methods, 91*(1), 93–100.
51. Sanchez, S. A., Tricerri, M. A., & Gratton, E. (2012). Laurdan generalized polarization fluctuations measures membrane packing micro-heterogeneity in vivo. *Proceedings of the National Academy of Sciences USA, 109*(19), 7314–7319.
52. Ionescu, D., & Ganea, C. (2012). A study of quercetin effects on phospholipid membranes containing cholesterol using Laurdan fluorescence. *European Biophysics Journal, 41*(3), 307–318.
53. Weber, P., Wagner, M., & Schneckenburger, H. (2010). Fluorescence imaging of membrane dynamics in living cells. *Journal of Biomedial Optics, 15*(4), 046017.
54. Dodes Traian, M. M., González Flecha, F. L., & Levi, V. (2012). Imaging lipid lateral organization in membranes with C-laurdan in a confocal microscope. *Journal of Lipid Research, 53*(3), 609–616.
55. M'Baye, G., Mély, Y., Duportail, G., & Klymchenko, A. S. (2008). Liquid ordered and gel phases of lipid bilayers: Fluorescent probes reveal close fluidity but different hydration. *Biophysical Journal, 3*, 1217–1225.
56. Kahn, E., Baarine, M., Dauphin, A., Ragot, K., Tissot, N., Seguin, A., et al. (2011). Impact of 7-ketocholesterol and very long chain fatty acids on oligodendrocyte lipid membrane organization: evaluation via LAURDAN and FAMIS spectral image analysis. *Cytometry Part A, 79*(4), 293–305.
57. Lúcio, A. D., Vequi-Suplicy, C. C., Fernandez, R. M., & Lamy, M. T. (2010). Laurdan spectrum decomposition as a tool for the analysis of surface bilayer structure and polarity: A study with DMPG, peptides and cholesterol. *Journal of fluorescence, 20*(2), 473–482.
58. Antollini, S. S., & Barrantes, F. J. (2007). Laurdan studies of membrane lipid-nicotinic acetylcholine receptor protein interactions. *Methods in Molecular Biology, 400*, 531–542. Review.
59. De Vequi-Suplicy, C. C., Benatti, C. R., & Lamy, M. T. (2006). Laurdan in fluid bilayers: Position and structural sensitivity. *Journal of fluorescence, 16*(3), 431–439.
60. Picardi, M. V., Cruz, A., Orellana, G., & Pérez-Gil, J. (2011). Phospholipid packing and hydration in pulmonary surfactant membranes and films as sensed by LAURDAN. *Biochimica et Biophysica Acta, 1808*(3), 696–705. gruppo 10.
61. Kim, H. M., Choo, H. J., Jung, S. Y., Ko, Y. G., Park, W. H., Jeon, S. J., et al. (2007). A two-photon fluorescent probe for lipid raft imaging: C-laurdan. *ChemBioChem, 8*(5), 553–559.
62. Vest, R., Wallis, R., Jensen, L. B., Haws, A. C., Callister, J., Brimhall, B., et al. (2006). Use of steady-state laurdan fluorescence to detect changes in liquid ordered phases in human erythrocyte membranes. *Journal of Membrane Biology, 211*(1), 15–25.
63. Zhang, Y. L., Frangos, J. A., & Chachisvilis, M. (2006). Laurdan fluorescence senses mechanical strain in the lipid bilayer membrane. *Biochemical and Biophysical Research Communications, 347*(3), 838–841.
64. Gaus, K., Zech, T., & Harder, T. (2006). Visualizing membrane microdomains by Laurdan 2-photon microscopy. *Molecular Membrane Biology, 23*(1), 41–48. Review.
65. Harris, F. M., Best, K. B., & Bell, J. D. (2002). Use of laurdan fluorescence intensity and polarization to distinguish between changes in membrane fluidity and phospholipid order. *Biochimica et Biophysica Acta, S1565*(1), 123–128.
66. Digman, M. A., Caiolfa, V. R., Zamai, M., & Gratton, E. (2008). The phasor approach to fluorescence lifetime imaging analysis. *Biophysical Journal, 94*(2), L14–L16.
67. Stefl, M., James, N. G., Ross, J. A., & Jameson, D. M. (2011). Applications of phasors to in vitro time-resolved fluorescence measurements. *Analytical Biochemistry, 410*(1), 62–69.
68. Zhou, Y., Wu, L., Wang, Q., & Wang, Y. (2011). Global analysis of dynamic fluorescence anisotropy by a polarized phasor approach. *Journal of fluorescence, 21*(1), 11–15.
69. Fereidouni, F., Bader, A. N., & Gerritsen, H. C. (2012). Spectral phasor analysis allows rapid and reliable unmixing of fluorescence microscopy spectral images. *Optics Express, 20*(12), 12729–12741.
70. Chen, L. C., Lloyd, W. R, 3rd, Chang, C. W., Sud, D., & Mycek, M. A. (2013). Fluorescence lifetime imaging microscopy for quantitative biological imaging. *Methods in Cell Biology, 114*, 457–488.
71. van Meer, G. (1998). Lipids of the Golgi membrane. *Trends in Cell Biology, 8*, 29–33.
72. Hao, M., Lin, S. X., Karylowski, O. J., Wustner, D., McGraw, T. E., & Maxfield, F. R. (2002). Vesicular and non-vesicular sterol transport in living cells. The endocytic recycling compartment is a major sterol storage organelle. *Journal of Biological Chemistry, 277*, 609–617.